AGU 100 ADVANCING EARTH AND SPACE SCIENCE | **FALL MEETING** San Francisco, CA | 9–13 December 2019

**T51F-0352**

# Characterization of porosity in the sediments entering the Northern Hikurangi Margin from Cation Exchange Capacity and IODP Expeditions 372 and 375 data : implications for compaction state, stress and fluid pressure

**Jade DUTILLEUL***, Sylvain BOURLANGE, Yves GÉRAUD, University of Lorraine, CNRS, GeoRessources, F-54000 Nancy, France
* : jade.dutilleul@univ-lorraine.fr ; *https://orcid.org/0000-0003-2961-077X*

IODP INTERNATIONAL OCEAN DISCOVERY PROGRAM | IODP FRANCE | GeoRessources | UNIVERSITÉ DE LORRAINE

## Geological context : the Northern Hikurangi Margin, New Zealand

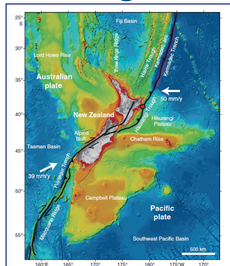


↑ **Fig. 1 : Tectonic map of New Zealand (Barnes *et al.*, 2019).** The red dot shows the location of Fig 2.

In 2017-2018, **IODP Expeditions 372 and 375** drilled several sites in the Northern Hikurangi margin, New Zealand, where **tsunami earthquakes** occurred in 1947 and shallow **Slow Slip Events** (SSEs) recur every 1 or 2 years, providing samples and *in situ* measurements to characterize the lithological, physical, thermal, chemical, hydrogeological and mechanical properties of the sediments in the basin entering the subduction zone and in the upper part of the accretionary prism. This extraordinary dataset allows to **investigate** the **processes triggering spatial and temporal transitions between** these **different fault slip styles**, including **excess pore pressure** through its control on effective normal stress. Excess pore pressure typically results from the ineffectual dewatering of low-permeability undercompacted sediments that tends to prevent consolidation.

We use porosity data to **characterize sediment compaction state** and any implications for stress and pore pressure at 2 sites :

- **Site U1520**, drilled through the top of the subducting Hikurangi Plateau and the overlying sedimentary cover composed by siliciclastic trench sediments above pelagic carbonate formations (**Fig. 6**);
- **Site U1518**, drilled through siliciclastic sediments equivalent to siliclastic units at Site U1520 in the frontal wedge to penetrate the Papaku thrust fault, a splay-fault expected to host SSEs (**Fig. 8**).

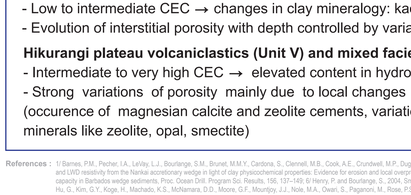


↑ **Fig. 3 : Zoom in of the frontal accretionary wedge where Site U1518 is located (Fagereng *et al.*, 2019).**

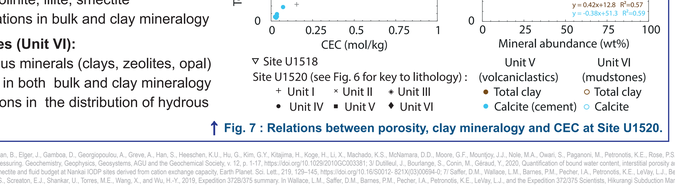


↑ **Fig. 2 : Seismic profile across North Hikurangi margin showing the location of Sites U1520 (~95 km from shore) and U1518 (~62 km from shore) drilled during IODP Expeditions 372-375 (Saffer *et al.*, 2019).**

## Site U1520 : Input sedimentary section

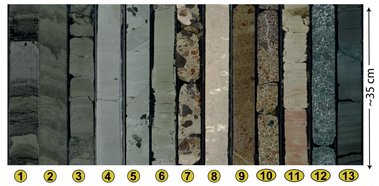


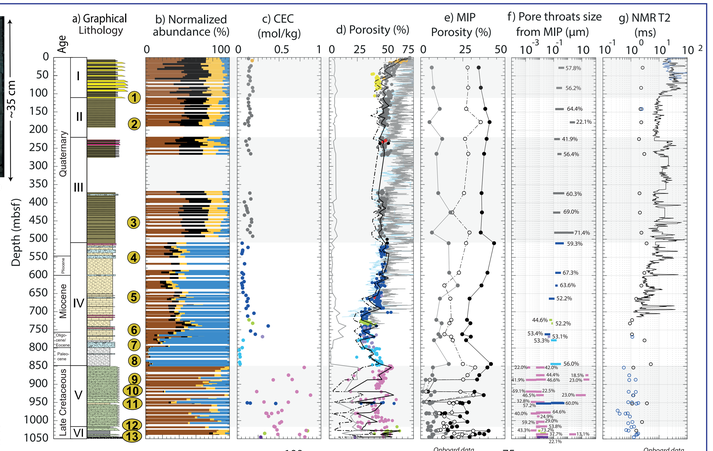


↑ **Fig. 6 : Summary of lithological (after Barnes *et al.*, 2019) and porosity data at reference Site U1520.**

**Key to lithology:**

c/d/f) a)
- Hemipelagic mud(stone)
- Sand(stone), clayey sand(stone)
- Silt(stone), silty sand(stone)
- Black mudstone
- Volcanic ash/tuff
- Volcaniclastic conglomerate
- Debris flow deposit
- Marl
- Calcareous mudstone
- Chalk, muddy chalk
- Basalt

b)
- Clay
- Quartz
- Feldspath
- Calcite

**Key to physical properties:**

d)
- Onboard porosity

Logging porosity :
- NMR
- Neutron

Porosity (this study) :
- Total
- Interstitial
- Bound water content

e)
- MIP porosity
- Trapped MIP porosity
- Free MIP porosity

g)
- T2 U1520A (logging)
- T2 U1520B (logging)
- T2 Laboratory 20 MHz
- T2 Laboratory 10 MHz

**Siliclastic Units I, II and III:**
- Low and constant CEC → homogeneous clay mineralogy: kaolinite, illite
- Normal consolidation: $\phi_i = 45.3\ exp(-0.041*\sigma')$ usable as reference trend at Site U1518

**Pelagic carbonate Unit IV:**
- Low to intermediate CEC → changes in clay mineralogy: kaolinite, illite, smectite
- Evolution of interstitial porosity with depth controlled by variations in bulk and clay mineralogy

**Hikurangi plateau volcaniclastics (Unit V) and mixed facies (Unit VI):**
- Intermediate to very high CEC → elevated content in hydrous minerals (clays, zeolites, opal)
- Strong variations of porosity mainly due to local changes in both bulk and clay mineralogy (occurence of magnesian calcite and zeolite cements, variations in the distribution of hydrous minerals like zeolite, opal, smectite)

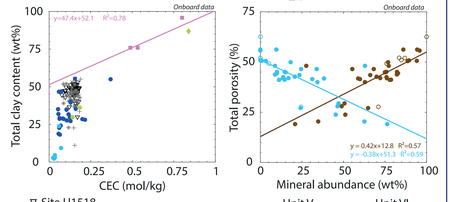


Site U1518
Site U1520 (see Fig. 6 for key to lithology) :
Unit I, Unit II, Unit III, Unit IV, Unit V, Unit VI

| Unit V (volcaniclastics) | Unit VI (mudstones) |
|---|---|
| Total clay | Total clay |
| Calcite (cement) | Calcite |

↑ **Fig. 7 : Relations between porosity, clay mineralogy and CEC at Site U1520.**

## Method : Correcting total porosity from clay-bound water to draw compaction curves

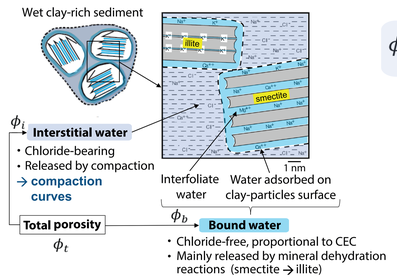


↑ **Fig. 4 : Zoom in of the total water content of a clay-rich sample saturated with seawater (modified after Conin *et al.*, 2011 and Salles *et al.*, 2008)**

$$\phi_i = \phi_t - \phi_b = \phi_t - n\,\frac{M_w}{\rho_w}\,CEC\,\rho_g(1-\phi_t)$$

where :
- $\phi_t$ is total porosity routinely measured onboard
- $\phi_b$ is bound water content
- $n$ is the number of molecule per CEC (n=15, **Fig. 5**)
- $M_w$ is the water molar mass (0.018 kg/mol)
- $\rho_w$ is the water density (1024 kg/m3)
- $CEC$ is the Cation Exchange Capacity (mol/kg)
- $\rho_g$ is the grain density (kg/m3)

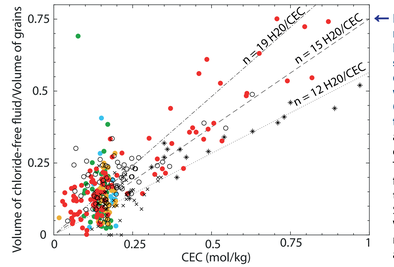


← **Fig. 5 : Bound water ratio versus CEC for Expeditions 372/375 samples allowing to determine the n = 15 water molecules per CEC trend used in this study.** The data are also compared to data from the litterature. The samples deviating from the n=15 H20/CEC trend are samples from Site U1520 Units V and VI that are particularly rich in smectite, but also zeolite and opal.

Hikurangi (this study) : U1517, U1518, U1519, U1520
Sumatra U1480, U1481 (Dutilleul *et al.*, 2020)
Barbados (Henry, 1997)
Nankai Upper and Lower Shikoku Basin (Henry and Bourlange, 2004) and Kumano Basin at Site C0001 (Conin *et al.*, 2011)

## Site U1518 : The Papaku thrust fault

**Key to lithology:**

c/d/f) a)
- Mud(stone)
- Fine sand(stone)
- Silty clay(stone)
- Sandy silt(stone)
- Volcanic ash
- Contorted

b)
- Clay
- Quartz
- Feldspath
- Calcite

**Key to physical properties:**

d)
- Onboard porosity

Logging porosity :
- NMR
- Neutron

Porosity (this study) :
- Total
- Interstitial
- Bound water content

e)
- MIP porosity
- Trapped MIP porosity
- Free MIP porosity

g)
- T2 U1518A (logging)
- T2 U1518B (logging)
- T2 Laboratory 20 MHz

**Key to structure:**

a)
1. Folded and faulted hanging-wall
2. Main brittle fault zone
3. Gradually decreasing brittle-ductiledeformation
4. Subsidiary fault zone
5. Less deformed footwall

2b. Breccias and locally fractured flow banding
2c. Breccia
2d. Truncated silt beds
2f. Flow banding

h)
- Normal fault
- Reverse fault
- Indeterminate fault
- Open fracture
- Filled fracture

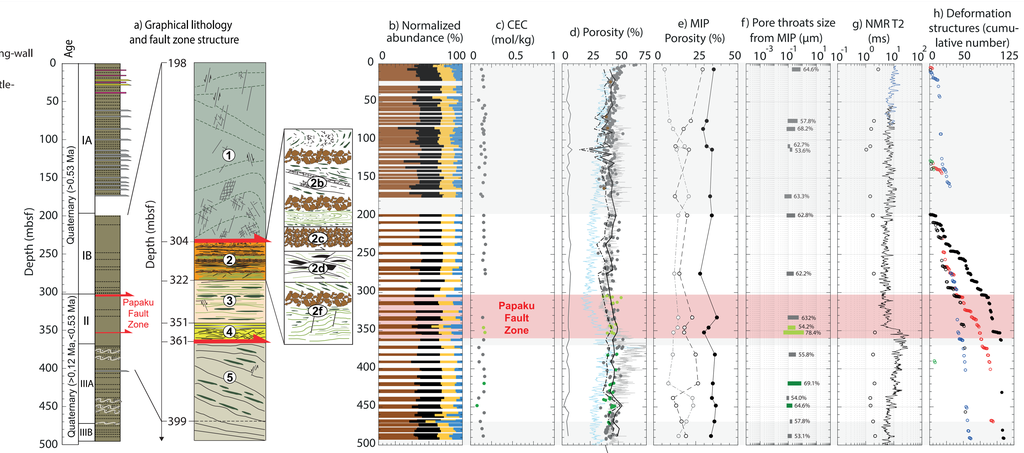


↑ **Fig. 8 : Summary of lithological (after Saffer *et al.*, 2019), structural (after Fagereng *et al.*, 2019) and porosity data at reference Site U1518.**

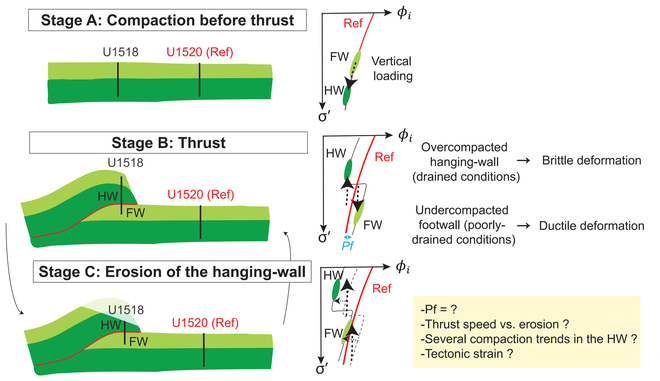


↑ **Fig. 11 : Example of model resulting in an interstitial porosity profile similar to that of U1518.**

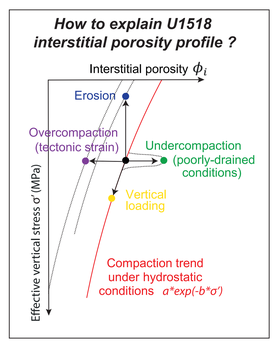


↑ **Fig. 10 : Cartoon explaining theoretical shift of interstitial porosity due to tectonic or hydrologic processes (modified after Conin *et al.*, 2011).**

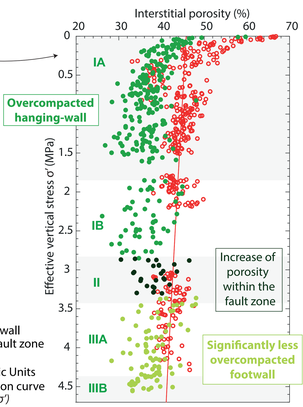


- U1518 hanging-wall
- U1518 Papaku fault zone
- U1518 footwall
- U1520 siliciclastic Units
- U1520 compaction curve $45.3\ exp(-0.041*\sigma')$

↑ **Fig. 9 : Comparison of interstitial porosity data at Site U1518 and reference Site U1520.** Interstitial porosity data used here is onboard total porosity data corrected from the average bound water content per unit.

**References :** 1/ Barnes, P.M., Pecher, I.A., LeVay, L.J., Bourlange, S.M., Brunet, M.M.Y., Cardona, S., Clennell, M.B., Cook, A.E., Crundwell, M.P., Dugan, B., Elger, J., Gamboa, D., Georgopoulou, A., Greve, A., Han, S., Heeschen, K.U., Hu, G., Kim, G.Y., Kitajima, H., Kluge, M., Li, X., Machado, K.S., McNamara, D.D., Moore, G.F., Mountjoy, J.J., Nole, M.A., Owari, S., Pagaran, M., Petronotis, K.E., Rose, P.S., Screaton, E.J., Shankar, U., Shepherd, C.L., Torres, M.E., Underwood, M.B., Wang, X., Woodhouse, A.D., and Wu, H.-Y., 2019, Site U1517. In Pecher, I.A., Barnes, P.M., LeVay, L.J., and the Expedition 372A Scientists, Creeping Gas Hydrate Slides - Proceedings of the International Ocean Discovery Program, 372A: College Station, TX (International Ocean Discovery Program). https://doi.org/10.14379/iodp.proc.372A.103.2019; 2/ Conin, M., Henry, P., Bourlange, S., Raimbourg, H. and Kreulchit, T., 2011, Interpretation of porosity and LWD resistivity from the Nankai accretionary wedge in light of clay physicochemical properties: Evidence for erosion and local overpressuring: Geochemistry, Geophysics, Geosystems, AGU and the Geochemical Society, v. 12, p. 1-17, https://doi.org/10.1029/2010GC003381; 3/ Dutilleul, J., Bourlange, S., Conin, M., Géraud, Y., 2020, Quantification of bound water content, interstitial porosity and fracture porosity in the sediments entering the North Sumatra subduction zone from Cation Exchange Capacity and IODP Expedition 362 resistivity data. Marine and Petroleum Geology, v. 111, p. 156-165, https://doi.org/10.1016/j.marpetgeo.2019.08.007; 4/ Fagereng, A., et al., 2019, Mixed deformation styles observed on a shallow subduction thrust, Hikurangi margin, New Zealand, Geology, v. 47, p. 1–5, https://doi.org/10.1130/ G45367.1; 5/ Henry, P., 1997, Relationship between porosity, electrical conductivity and cation exchange capacity in Barbados wedge sediments. Proc. Ocean Drill. Program Sci. Results, 156, 137–149; 6/ Henry, P. and Bourlange, S., 2004, Smectite and fluid budget at Nankai IODP sites derived from cation exchange capacity, Earth Planet. Sci. Lett., 219, 129–145, https://doi.org/10.1016/S0012- 821X(03)00694-0; 7/ Saffer, D.M., Wallace, L.M., Barnes, P.M., Pecher, I.A., Petronotis, K.E., LeVay, L.J., Bell, R.E., Crundwell, M.P., Engelmann de Oliveira, C.H., Fagereng, A., Fulton, P.M., Greve, A., Harris, R.N., Hashimoto, Y., Hupers, A., Ikari, M.J., Ito, Y., Kitajima, H., Kutterolf, S., Lee, H., Li, X., Luo, M., Malie, P.R., Meneghini, F., Morgan, J.K., Noda, A., Rabinowitz, H.S., Savage, H.M., Shepherd, C.L., Shreedharan, S., Solomon, E.A., Underwood, M.B., Wang, M., Woodhouse, A.D., Bourlange, S.M., Brunet, M.M.Y., Cardona, S., Clennell, M.B., Cook, A.E., Dugan, B., Elger, J., Gamboa, D., Georgopoulou, A., Han, S., Heeschen, K.U., Hu, G., Kim, G.Y., Kopf, A., Machado, K.S., McNamara, D.D., Moore, G.F., Mountjoy, J.J., Nole, M.A., Owari, S., Pagaran, M., Rose, P.S., Screaton, E.J., Shankar, U., Torres, M.E., Wang, X., and Wu, H.-Y., 2019, Expedition 372/375 summary. In Wallace, L.M., Saffer, D.M., Barnes, P.M., Pecher, I.A., Petronotis, K.E., LeVay, L.J., and the Expedition 372/375 Scientists, Hikurangi Subduction Margin Coring, Logging, and Observatories: Proceedings of the International Ocean Discovery Program, 372B/375: College Station, TX (International Ocean Discovery Program), https://doi.org/10.14379/iodp.proc.372B375.101.2019; 8/ Salles, F., Beurrotes, I., Bildstein, O., Jullien, M., Raynal, J., Denoyel, R., Van Damme, H., 2008, A calorimetric study of mesoscopic swelling and hydration sequence in solid Na-montmorillonite, Applied Clay Science, v.39, p. 186-201, https://doi.org/10.1016/j.clay.2007.06.001.

**Acknowledgements :** We greatly acknowledge CNRS-INSU and IODP-France for funding this research. We also thank David Billet, Philippe Rousselle, Maximilien Beuret, Valérie Goncalves, Géraldine Kitzinger and Hervé Marmier from the LIEC laboratory (Nancy and Metz, France) where all CEC, exchangeable cation composition and soluble chloride content measurements were done, and Didier Stemmelen from the LEMTA laboratory (Nancy, France) for his support in NMR analyses.

**Data :** This research used data provided by the International Ocean Discovery Program (IODP) and freely available on the LIMS Report Interface Page at web.iodp.tamu.edu/LORE or on the log database at mtp.ldeo.columbia.edu/logdb/scientific_ocean_drilling. CEC, exchangeable cation composition, soluble chloride content, interstitial porosity, bound water content, NMR and mercury porosity data will be available in the OTELo Research Data Repository (*https://ordar.otelo.univ-lorraine.fr*).